Proceedings of the ASME 2010 3rd Joint US-European Fluids Engineering Summer Meeting and 8th International Conference on Nanochannels, Microchannels, and Minichannels
FEDSM-ICNMM2010
August 1-5, 2010, Montreal, Canada

FEDSM-ICNMM2010-30541

VIBRATION RESPONSE BEHAVIOUR OF A HIGH SOLIDITY, LOW ROTATIONAL VELOCITY, VERTICAL AXIS WIND TURBINE

Kevin W. McLaren
McMaster University
Mechanical Engineering
1280 Main Street West,
Hamilton, Ontario,
L8S4L8, Canada
905-525-9140 x 24544
mclarekw@mcmaster.ca

Stephen W. Tullis
McMaster University
Mechanical Engineering
1280 Main Street West,
Hamilton, Ontario,
L8S4L8, Canada
905-525-9140 x 27692
stullis@mcmaster.ca

Samir Ziada
McMaster University
Mechanical Engineering
1280 Main Street West,
Hamilton, Ontario,
L8S4L8, Canada
905-525-9140 x 27530
ziadas@mcmaster.ca

ABSTRACT

A series of full scale experimental wind tunnel tests were performed to determine the aerodynamic loading behaviour on the airfoils of a high solidity, low rotational velocity, 3 bladed H-type vertical axis wind turbine. The primary vibration response was resonance excitation of the dominant whirling mode of the turbine. However, for a significant number of test cases, resonance behaviour was also observed in the bending strains of the airfoil support struts, primarily corresponding to higher natural frequencies. Furthermore, under various test conditions, vibration amplitude within the support struts was observed to change dramatically during a single test run, suggesting that the vibration was jumping between sets of airfoil support struts in a complex beating mode. In order to isolate the numerous vibration excitation and response behaviours, tests were performed over a range of flow velocities from 8 m/s to 11 m/s with two different support shaft end conditions.

INTRODUCTION

The increasing prevalence of Vertical Axis Wind Turbines (VAWT) has renewed interest in studying numerous aspects of their long-term operation; including vibration excitation, and response behaviour. The fatigue life of a VAWT is often considered as equally important as power output due to its substantial impact on the cost effectiveness of a wind turbine system [1]. As such, the current research endeavours to build upon previous experimental studies [2,3] to further the fundamental understanding of aerodynamic loading, and thus vibration excitation and noise generation. A particular emphasis will be given to high solidity (Solidity ratio, $\sigma = Nc/2R = 0.43$), low rotational velocity (30 RPM to 160 RPM) VAWT designs where dynamic stall effects are dominant.

In order to facilitate this study, aerodynamic loading and vibration measurement techniques were devised and employed on a full-scale VAWT prototype. Ultimately, the effect of changes in blade shape, size, number and mounting configuration can be tested and a selection can be made in order to minimize vibration loading while maximizing power output. The particular turbine under investigation will be produced and marketed as a small scale rooftop power unit for urban areas. As a result, the undertaking of this research is crucial due to the potential impact of structural vibration of the turbine and building, noise generation and fatigue failure, on the local population.

NOMENCLATURE

H – Turbine Height [m]
N – Number of Turbine Blades [-]
R – Turbine Radius [m]
$U_{incident}$ – Incident Wind Velocity [m/s]
$U_{rotation}$ – Wind Velocity due to Rotation [m/s]
U_{wind} – Ambient Wind Velocity [m/s]
c – Airfoil Chord Length [m]
n – Positive Integer, 1, 2, 3 ... [-]
α – Relative Angle of Attack [Deg]
θ – Angle of Rotation [Deg]
λ – Blade Speed Ratio [-]
ρ – Air Density [kg/m^3]
σ – Solidity Ratio [-]
ω – Rotational Velocity [Rev/min]

MOTIVATION

A series of full scale experimental wind tunnel tests were performed on a high solidity, 3 bladed H-type vertical axis wind turbine prototype to determine the aerodynamic loading behaviour on the airfoils. The vertical axis wind turbine under investigation is a lift type design, such that the power output is produced through the lift force generated on the surface of the airfoils. As the turbine rotates the airfoils encounter an incident wind velocity that is the vector summation of the ambient flow velocity and the flow velocity due to turbine rotation (Fig. 1). This flow velocity approaches the airfoils at a relative angle of attack, α, resulting in a thrust force tangential to the rotational path and a radial force. The wind tunnel flow velocity in this study is relatively constant such that the radial load is the primary source of vibration excitation while the thrust load is mainly power producing. Under normal operating conditions however, large variations in atmospheric wind velocity play an important role in vibration excitation.

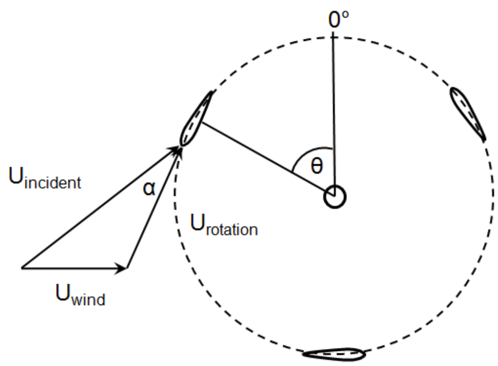

Figure 1: Vertical axis wind turbine principal of operation.

One of the unique features of the turbine is its uncharacteristically large airfoils relative to the overall size of the turbine. Because of the relatively high solidity of this particular wind turbine design, it operates at very low rotational velocity relative to the ambient flow velocity. This ratio of the rotational velocity of the wind turbine to the ambient flow velocity is the blade speed ratio, $\lambda = (2\pi/60)*(\omega R/U_{wind})$, and is the defining characteristic for determining the potential for dynamic stall. Dynamic stall is a non-linear unsteady aerodynamic effect that occurs when the pitch angle of an airfoil is rapidly changed. This motion often causes strong vortices to be shed from the surface of the airfoil. These vortices briefly increase the lift produced by the airfoil, however, as soon as they pass behind the trailing edge, the lift reduces dramatically. This cyclic loading and unloading of the turbine airfoils is expected to be a strong source of vibration excitation and is the primary motivation for this study.

For very low blade speed ratios ($\lambda > 1.5$) the turbine airfoils will be subjected to very high relative angles of attack on the order of ±40° or greater, promoting dynamic stall and the production of large scale vortex structures. While, for blade speed ratios greater than 5.0 the relative angle of attack will be limited to at most ±12°, and the onset and severity of dynamic stall will be greatly suppressed. At these high blade speed ratios it is the secondary effects such as blade shape, support struts and the rotating shaft that dominate the turbine aerodynamics, and thus turbine loading [4].

Based upon a series of computational fluid dynamic (CFD) simulations of a VAWT cross-section performed by McLaren et al. [5], the expected thrust and radial loading characteristics over a range of blade speed ratios can be explored (Fig. 2). While the CFD simulations do not incorporate three-dimensional flow effects, the aerodynamics and stall characteristics of the airfoils are fairly well represented, as was demonstrated through flow visualization by Fiedler & Tullis [6]. However, because of the two-dimensional nature of the CFD model, power output predictions exceed those observed experimentally [7]. The most striking feature of the expected loading curves is the large peak in thrust and radial force on the upstream pass ($0° \leq \theta \leq 180°$) as the airfoil lift force increases along with the relative angle of attack, followed by dynamic stall. From Fig. 2 it is also apparent that the vibration exciting radial load amplitude is typically on the order of five times greater than that of the power producing thrust load.

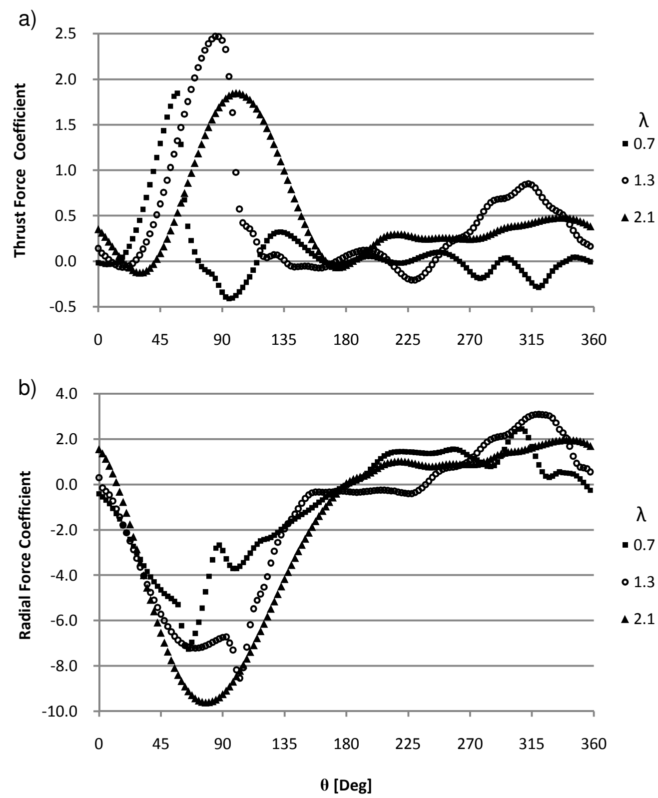

Figure 2: Expected (a) thrust, and (b) radial force coefficients, obtained from 2D CFD simulations [5].

From Fig. 2 it is clear that for the very low blade speed ratio of 0.7, due to the high relative angle of attack and pitch rate at which the airfoil is being driven, the onset of dynamic stall occurs early on in the rotation and maximum thrust and radial loads are attained at just 55° of rotation. For the remainder of the rotation, the CFD simulation predicts that a number of smaller vortices are shed from the airfoil, resulting in thrust loading oscillations of various durations at a rate of approx. 6 cycles per revolution. For a moderate blade speed ratio of 1.3, the onset of dynamic stall is delayed and maximum thrust and radial loading are significantly larger and occur near 85° of rotation. Here loading is applied at a frequency of approx. 3 cycles per revolution for each of the turbine airfoils. For a relatively large blade speed ratio of 2.1, the CFD simulations indicate that dynamic stall is greatly suppressed and the upstream peak in thrust loading is attained gradually and even further into the rotation than either of the lower blade speed ratio cases ($\theta \approx 100°$).

By performing a summation of the loading from each blade, the total aerodynamic load being applied to the turbine in both the streamwise and cross-stream directions as a function of the angle of rotation can then be determined from the CFD predictions (Fig. 3). From Fig. 3 some important characteristics of the nature of the net turbine loading can be determined from these numerical predictions. First, it is anticipated that, independent of the blade speed ratio, the net load on the turbine will be applied at a rate of three cycles per revolution or the "blade pass frequency". Second, the streamwise and cross-stream loading are typically out of phase by 30 to 40 degrees of rotation, indicating that the turbine will be highly susceptible to excitation of the primary whirl mode. Finally, for low blade speed ratios the load application and removal is sudden and abrupt, while for high blade speed ratios the load application is nearly sinusoidal.

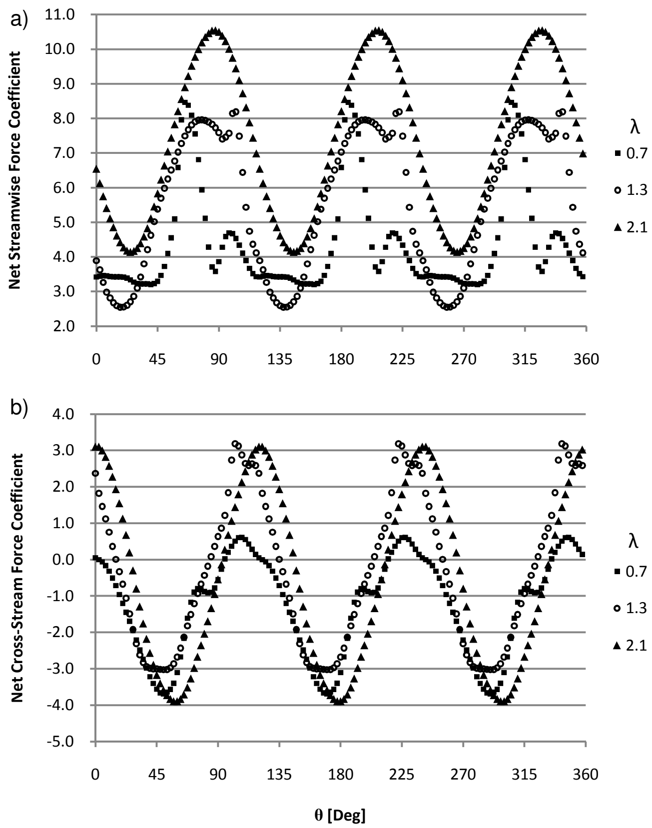

Figure 3: Expected net (a) streamwise, and (b) cross-stream force coefficients, obtained from 2D CFD simulations [5].

EXPERIMENTAL SET-UP

The open loop wind tunnel employed to perform the current study is located at the University of Waterloo Fire Research Facility in Ontario, Canada. The wind tunnel consists of a 20 metre long test enclosure with an 8 metre wide by 6 metre high inlet. An array of six 75 kW vane axial fans arranged in 2 rows, 3 wide drives the flow at velocities of upwards of 12 m/s. The flow from the 6 fans is initially conditioned through a pair of flow settling screens located 3.5 metres from the fan outlets as well as an array of flow straightening ducts at the plenum exit. For all test cases the turbine prototype was situated 8 metres downstream from the plenum exit where flow measurement calibration studies indicate a relatively uniform flow field (±8%). Further details of the wind tunnel and its operating conditions can be found in Devaud et al. [8]. For this study, wind speed was measured through the use of both a sonic and propeller type anemometer mounted at mid height of the turbine, both of which are accurate to ±2%. Special care was taken to ensure that the anemometers were not positioned in the wake of the flow straightening vanes.

The wind turbine itself consists of three straight blades 3 metres in length mounted at a radius of 1.4 metres. The airfoil profile is a symmetric NACA 0015 with a chord length of 450 mm truncated at the trailing edge to a final length of 420 mm. Figure 4 shows the wind turbine prototype mounted within the wind tunnel cross section.

The wind turbine rotational velocity was regulated (±1 RPM) by a simple closed-loop control system consisting of a disk brake and rotational frequency measurement. Through the use of a floating brake calliper and load cell, the net torque output of the wind turbine was also obtained. Due to the low thrust loading at low blade speed ratios and high aerodynamic and frictional losses at high blade speed ratios, operation of the turbine was limited to the range of 25 to 145 RPM where net power production is possible.

Figure 4: Wind turbine mounted within the wind tunnel. Highlighted region indicates the accelerometer mounting location. Note the sonic and propeller type anemometers located upstream of the turbine as well as the guy wire support system attached to the top of the turbine's stationary inner shaft.

In order to measure the vibration response of the turbine, two Kistler piezoelectric accelerometers (sensitivity of 0.2%) were magnetically mounted to the surface of the stationary support shaft extending out of the top of the turbine in the streamwise and cross-stream directions (Fig. 4). Also mounted to the stationary support shaft was a proximity sensor trigger pin used to indicate the angular position of the instrumented turbine struts. While not required under normal operating conditions, the extension to the stationary inner shaft of the turbine was manufactured in order to allow for the use of a guy wire support system. Mounted to the top of the inner shaft are a large eyebolt and a collection of high strength shackles to which the support guy wires can be attached (Fig. 4). The entire guy wire system consists of a set of six 3/8" (9.5 mm) cables fixed to the wind tunnel support structure at evenly spaced intervals of approximately 60°.

In order to measure the thrust and radial forces applied to the airfoils, three full Wheatstone bridges each consisting of four strain gauges, were mounted in small protective cavities within both the upper and lower support struts of a single blade (Fig. 5). Both the top and bottom strut were instrumented in order to measure the entire load being applied to the airfoil as well as the load distribution between the support struts. Due to the similarity of the vibration response from the two arms, and for the sake of clarity, this study will focus exclusively on the output of the bottom strut's set of Wheatstone bridges.

The Wheatstone bridges mounted closest to the shaft and at the mid-point of the strut were wired in such a manner that they were sensitive to bending in the horizontal plane and thus their output is primarily a function thrust loading and vertical torsion of the blade. The Wheatstone bridge closest to the blade was wired so as to be sensitive to tensile loading and as such produces an output which is primarily a function of the radial load. Through a set of calibration coefficients the output of theses sensors can be converted into the thrust and radial load components, as well as the vertical torsion component. Acceleration, position and strain measurements were all acquired at a sampling rate of 2048 Hz.

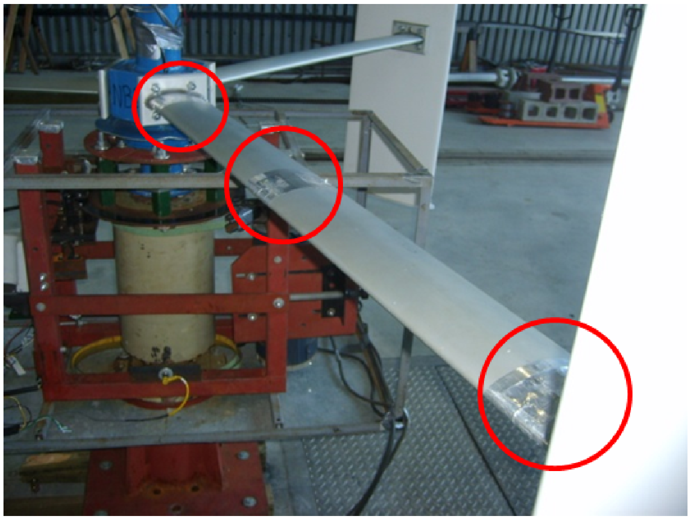

Figure 5: Bottom turbine support strut. Wheatstone bridges are mounted within the highlighted regions. The turbine blade is in the near field of the image on the extreme right side. Closest to the blade is the tension sensor, while at the mid-point of the strut and immediately next to the shaft are the horizontal bending moment sensor arrangements.

TEST RESULTS

Turbine Natural Frequency Characterization

In order to characterize the natural frequency response of the wind turbine both with and without the guy wire system in place, a series of impact hammer tests were performed. Due to the asymmetry of the turbine base support, as well as the effect of the turbine blade position on the system response, a set of 4 tests was run. Excitation in both the streamwise (X-Axis) and cross-stream (Y-Axis) directions was applied to the turbine shaft at the upper strut location, first with one of the blades aligned in the streamwise direction, then again with one of the blades aligned in the cross-stream direction. A summary of the results of these tests can be found in Table 1.

Table 1: Stationary turbine natural frequencies as determined from impact hammer tests

Without Cables [Hz]	With Cables [Hz]
4.03	6.38
4.34	6.81
9.03	9.69
	10.94
	13.06

For the test case without the cable system in place, the effect of the asymmetry of the turbine base support can clearly be seen in the twinning of the primary bending mode of the wind turbine at the closely spaced frequencies of 4.03 and 4.34 Hz. In addition, one of the higher strut modes, presumably due to blade bouncing, can also be seen at approx. 9 Hz. The most immediate effect of implementing the cable support system is to change the primary bending mode of the turbine from a fixed-free condition with streamwise and cross-stream frequencies of 4.03 and 4.34 Hz respectively, to a fixed-pinned condition with a streamwise frequency of 6.81 Hz and a cross-stream frequency of 6.38 Hz. In addition to this much anticipated effect, the immergence of two additional blade modes at considerably higher frequencies was observed. While the expected vibration excitation frequency range falls well below these higher blade mode natural frequencies, their effect on the vibration response of the turbine will be closely monitored along with the primary bending frequencies.

Primary Whirl Mode Excitation

The primary vibration response of the turbine was resonance excitation of the dominant whirling mode. Significant deflection of the support shaft was observed at coincidence of this first natural frequency of the turbine and the blade pass frequency at which the turbine was operating (Fig. 6).

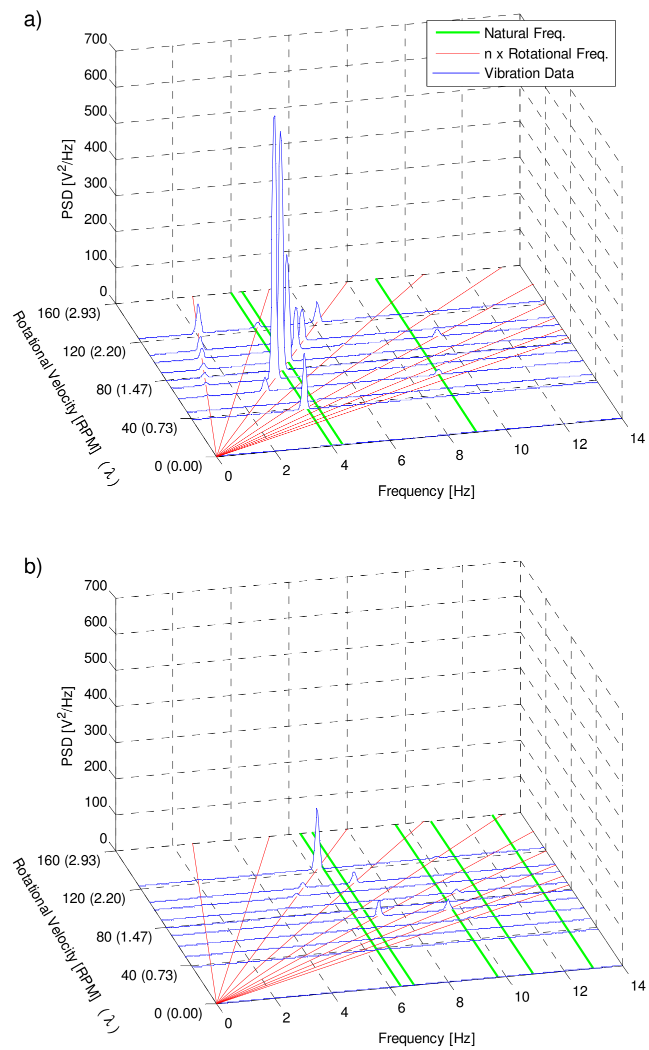

Figure 6: Power spectral density of turbine vibration as a function of rotational velocity in the streamwise direction for a flow velocity of 8 m/s. (a) without cables, (b) with cables. Green lines indicate natural frequencies obtained from the impact tests, while red lines are integer multiples of the rotational frequency.

Without the guy wire system attached the primary whirling frequency of the turbine is coincident with the blade pass frequency at 75 RPM. As per the power spectral density (PSD) of the turbine vibration in the streamwise direction this results in appreciable vibration excitation of the turbine over the typical power producing operating range of $1.4 \leq \lambda \leq 1.8$ (Fig. 6a). As expected, very little response is observed for the higher frequency mode of the turbine. Despite some differences in the net streamwise and cross-stream aerodynamic loading little difference is seen in the response of the turbine to each of these loading components. Therefore, the cross-stream vibration response is not presented. With the support cables in place, the primary structural mode of the turbine now coincides with the blade pass frequency at 135 RPM. While the first onset of a response to the whirling mode of the turbine is apparent at high RPM, little vibration response is seen throughout the typical operating range for any of the turbine modes identified by the impact hammer tests (Fig. 6b).

In order to gain a greater understanding of the vibration response of the turbine to the primary bending frequency, the normalized power spectral density amplitude for the blade pass frequency is calculated and plotted in Fig. 7. Because the amplitude of vibration is a function of the amount of power available in the oncoming flow, normalizing the power spectral density amplitude by the product of the dynamic pressure and the flow rate through the turbine ($^1/_2\rho U_{wind}{}^3 2RH$) results in a collapse of the data. Figure 7a clearly demonstrates the exponential growth in vibration amplitude up to the resonance frequency without the cable system attached.

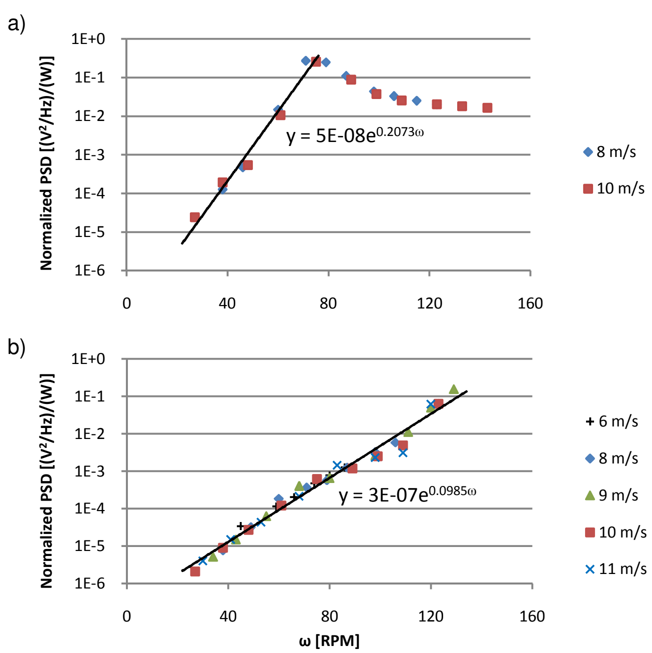

Figure 7: Power spectral density of the blade pass frequency normalized by the power available in the oncoming flow in the streamwise direction. (a) without cables, (b) with cables.

With the cable support system in place (Fig. 7b) the blade pass frequency amplitude is limited to the exponential growth region as the resonance frequency is at the upper limit of the operating capabilities of the wind turbine (Refer to Fig. 6b). This growth trend exists in both the streamwise and cross-stream directions. Note that with the cable system in place the growth rate of the response to the blade pass frequency is approximately one half of that observed without the cables attached. This is most likely due to the change in mode shape and the increase in energy required to excite the primary mode of the fixed-pinned shaft over the primary mode of the fixed-free shaft. A decrease in response amplitude due to the addition of the cables is likely a result of the fixed accelerometer location at approximately 3/4 of the height of the turbine (Refer to Fig. 4). Mounting the accelerometer at this location is mainly a function of the limited exposure of the stationary shaft and means that it is not at the position of maximum deflection or acceleration for either case.

Strut Mode Excitation

Strain gauges mounted to the surface of the airfoil support struts measured bending and tension strains produced by the aerodynamic airfoil loading. These sensors primarily provided information on the vibration response of the higher frequency structural modes.

Resonance: For a number of test cases, at coincidence of the strut mode natural frequencies with integer multiples of the rotational frequency of the turbine, the strain measurements became saturated with resonance response. This behaviour had a significant impact on the ability to ascertain the mean sensor output due to aerodynamic loading. As such, for each test case data was recorded for a minimum of 30 revolutions and averaged over the total number of revolutions to produce a mean value curve. This mean output signal was then subtracted from the raw data in order to produce an additional data set. This data set represents the superimposed vibration response of the sensors to the natural frequencies of the turbine.

In cases where there is no resonance response, this data set can be employed to determine the nature and severity of the excited vibration mode. From Fig. 8 it can be seen that the raw data is relatively consistent from one revolution to the next, and that the difference between the mean and raw data is at a fixed frequency. However, in cases with resonance, the response to the natural frequency of the support strut overwhelms the mean loading signal (Fig. 9). In this instance the difference between the mean and raw data sets is small and represents minor changes in amplitude and phase from one revolution to the next. Note the considerable change in mean strain amplitude from the relatively small deflections of the non-resonant test case to the appreciable vibration of the resonant test case.

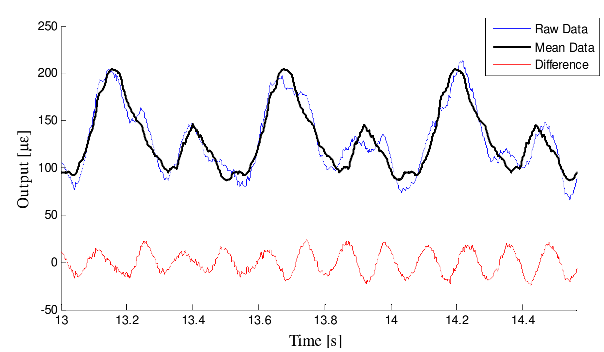

Figure 8: Sensor output for the strain gauge Wheatstone bridge mounted at the mid-point of the strut without the cable system attached. Three revolutions of the raw sensor data are shown along with the mean and superimposed vibration signals for a typical case without resonance (U_{wind}=8 m/s, ω=115 RPM, λ=2.1).

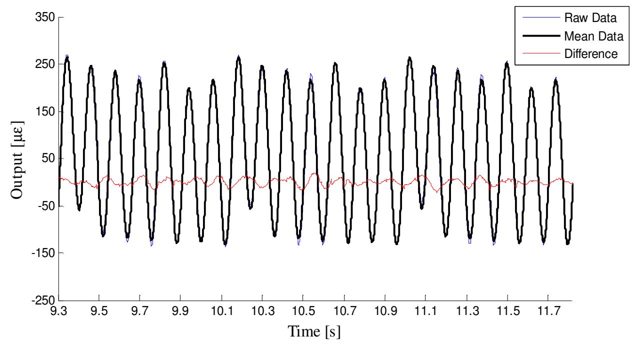

Figure 9: Sensor output for the strain gauge Wheatstone bridge mounted at the mid-point of the strut with the cable system attached. Three revolutions of the raw sensor data is shown along with the mean and superimposed vibration signals for a typical case with resonance (U_{wind}=8 m/s, ω=72 RPM, λ=1.3).

In order to better understand what modes are being excited, the PSD of the superimposed vibration data for the mid-strut bending moment sensor is calculated and plotted in Fig. 10. From this figure it is clear that the primary vibration response of the turbine struts occurs at coincidence of all integer multiples of the turbine rotational frequency with previously undefined natural frequencies of 8.1 and 8.5 Hz for test cases without cables and 8.3 and 8.7 Hz for test cases with cables. The fact that these modes did not appear in the impact hammer tests indicates that they are likely bending modes of the struts in the horizontal plane which would not be excited by impact loading of the entire turbine in the streamwise and cross-stream directions. Further investigation into the nature of these higher frequency structural modes is ongoing.

For cases without the cable system in place the primary whirling mode of the turbine does not appear in the strain gauge vibration response (Fig. 10a). However, for cases with the cable support system the whirling mode of the turbine is present. As can be seen in Fig. 10b, at zero rotational velocity there is a single primary natural frequency of the turbine at approximately 6.7 Hz. However, as the rotational velocity of the turbine is increased this natural frequency is split into two frequencies, presumably as a result of the gyroscopic effect.

The gyroscopic effect comes about as a result of the large moment of inertia of the turbine and the relatively low stiffness of the turbine base and cable supports. Whirl of the turbine generates a moment, the reaction of which acts on the support structure in addition to the stiffness of the system [9]. The lower frequency represents the circumstance where whirl of the turbine is opposed to rotation, thus lowering the effective system stiffness. While, the higher frequency represents the instance where the effective stiffness of the system is increased as the direction of whirl is the same as the direction of turbine rotation [9]. Typically speaking, backward whirl, where the direction of whirl and rotation are opposed, cannot be excited by the unbalance force of a simple isotropic system. However, in cases with asymmetric supports such as this it is more likely to occur [10].

Having characterized the natural frequency response of the turbine support struts themselves, analysis of the output of the sensors was performed. The first step in analysing the strain measurements was to determine which test cases display resonance characteristics by calculating the PSD of the raw data and searching for large amplitude responses.

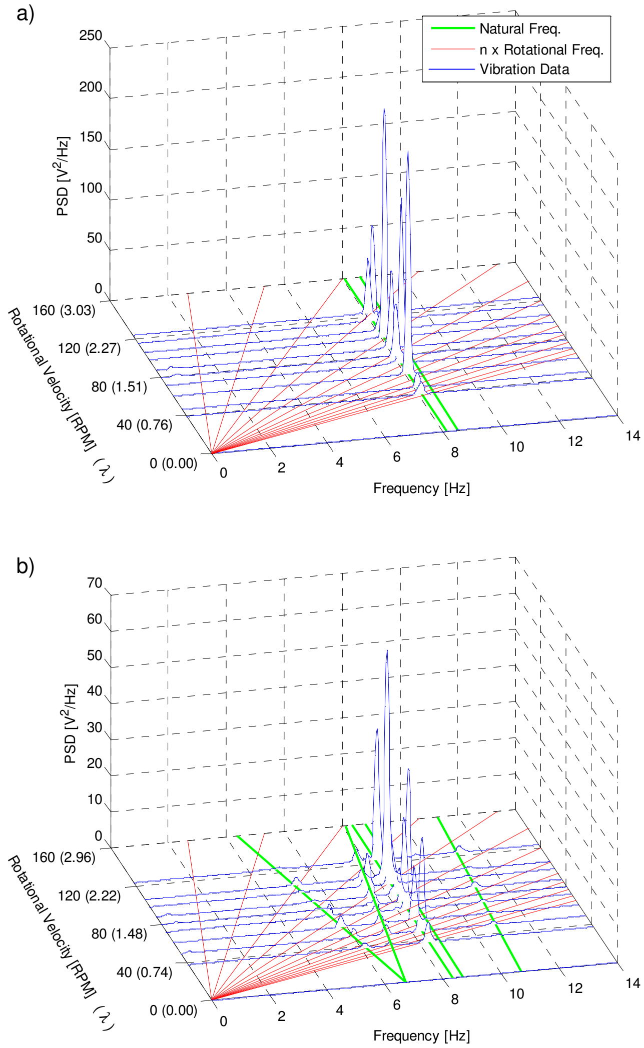

Figure 10: Power spectral density of the mid-strut bending moment sensor superimposed vibration data set as a function of rotational velocity for a flow velocity of 8 m/s. The 'superimposed vibration data set' refers to the difference between the raw and mean signal output. (a) without cables, (b) with cables. Green lines indicate frequencies with high vibration response, while red lines are integer multiples of the rotational frequency.

Figure 11 shows the response of the tension and mid-strut bending moment sensors without the cables attached at a wind velocity of 8 m/s. First and foremost, these figures display the considerable difference in the relative amplitude of response from each sensor. The tension sensor, wired to be responsive to tension rather than bending moment, has minimal response to the dominant natural frequencies of the struts. The mid-strut sensor however, being wired to measure bending strain in the horizontal plane, is very sensitive to this natural mode of vibration. As for all previous and subsequent cases, the behaviour of the shaft side bending moment sensor closely resembles that of the mid-strut bending moment sensor and as such has been omitted. Secondly, each of the sensors displays a response to the first and second multiples of the rotational frequency. Based upon the anticipated loading behaviour of the airfoils over a full rotation, this is entirely expected (Refer to Fig. 2). Finally, a strong response at 60 RPM and 100 RPM where λ=1.1 and λ=1.8 respectively, dominates the mid-strut sensor output.

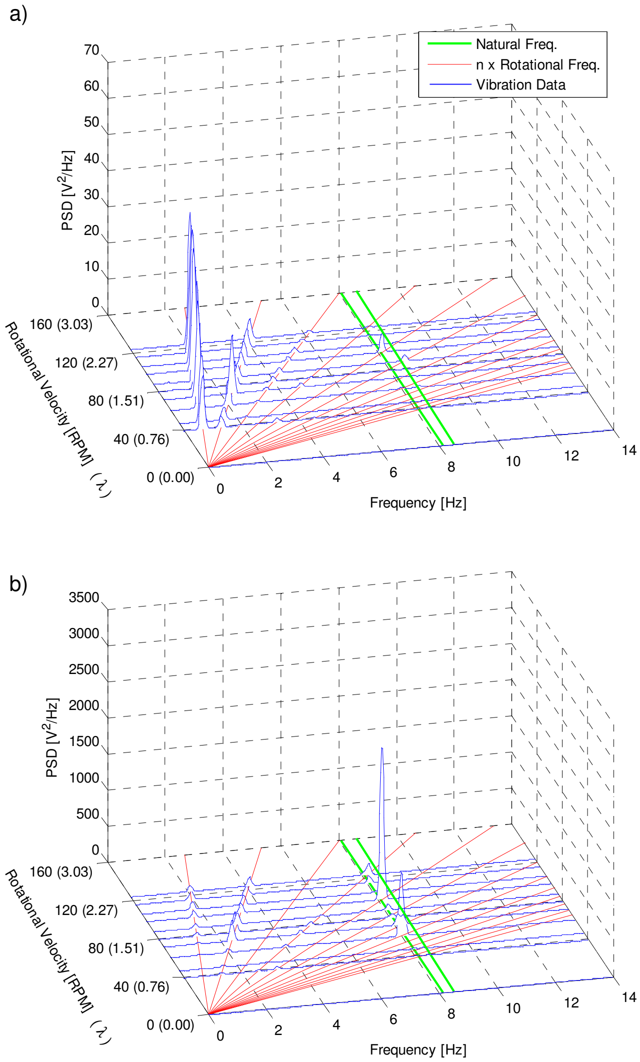

Figure 11: Power spectral density of the raw sensor data without cables as a function of rotational velocity for a flow velocity of 8 m/s. (a) tension sensor, (b) mid-strut bending moment sensor.

A sample of the raw and average strain measurements of the mid-strut bending moment and tension sensors provides a better understanding of the effect of this response on the load measurements. While not shown, for a very low blade speed ratio of 0.7 the mid-strut bending moment sensor that is proportional to thrust loading displays many of the expected characteristics (Refer to Fig. 2). A sharp increase in the thrust loading occurs on the upstream portion of the rotation, peaking at 55° of rotation. Following this is a series of lower amplitude fluctuations in thrust loading throughout the duration of the downstream portion of the rotation. Proportional to the radial force applied to the airfoil, the tension sensor output for λ=0.7 also reflects the expected loading behaviour (Refer to Fig. 2).

For a blade speed ratio of 1.1, a large spike in the vibration response for the bending moment sensor can be seen at a frequency of 8.1Hz (Fig. 11b). The response to this natural mode of vibration can clearly be seen in the bending strain measurement of the mid-strut sensor (Fig. 12a). While the vibration amplitude does vary quite considerably throughout the measurement period, the sensor is unmistakably responding to the 8th multiple of the rotational frequency. From a mean load measurement perspective this sample is practically unusable. Note the mean offset due to centrifugal loading in this and all subsequent tension sensor outputs (Fig. 12b).

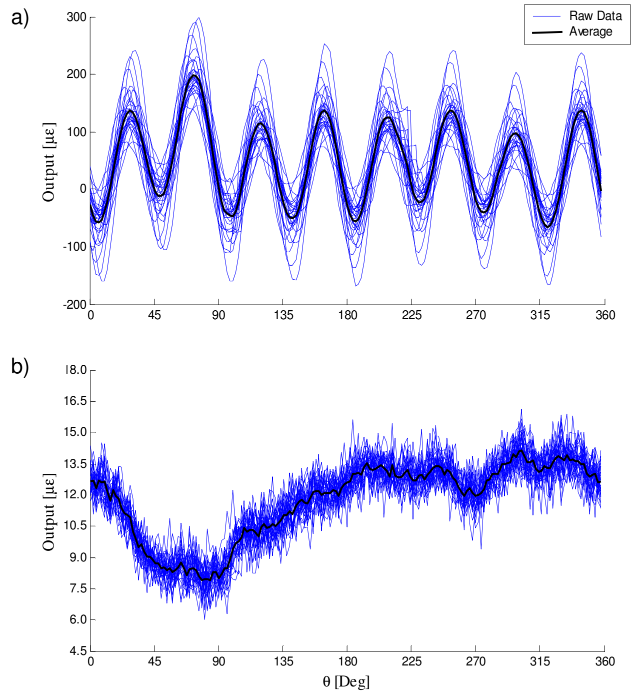

Figure 12: Raw and mean strain gauge sensor output as a function of the angle of turbine rotation without the cable system attached at a wind speed of 8 m/s. Raw data consists of a minimum of 30 revolutions of data. (a) mid-strut bending moment sensor, (b) tension sensor (ω=60 RPM, λ=1.1)

Proceeding to an intermediate blade speed ratio of 1.45, the delay in the onset and severity of dynamic stall on the upstream portion of the rotation can be observed as the maximum thrust and radial loading now occurs at 77° of rotation (Fig. 13). Furthermore, the existence of a second peak in loading on the downstream portion of the rotation indicates that as expected, pronounced dynamic stall has occurred once again only to a lesser degree. Again, the tensile strain closely resembles the expected loading behaviour with a marked increase in the mean loading component due to the increase in rotational velocity.

For a blade speed ratio of 1.8, resonance is once again encountered and response behaviour similar to a blade speed ratio of 1.1 is observed. However, in this instance it is the 5th multiple of the rotational frequency that coincides with the strut mode occurring at 8.1 Hz (Fig. 11b). In this particular test case the vibration excitation is so large that a response to it can even be seen in the tension sensor output (Fig. 11a).

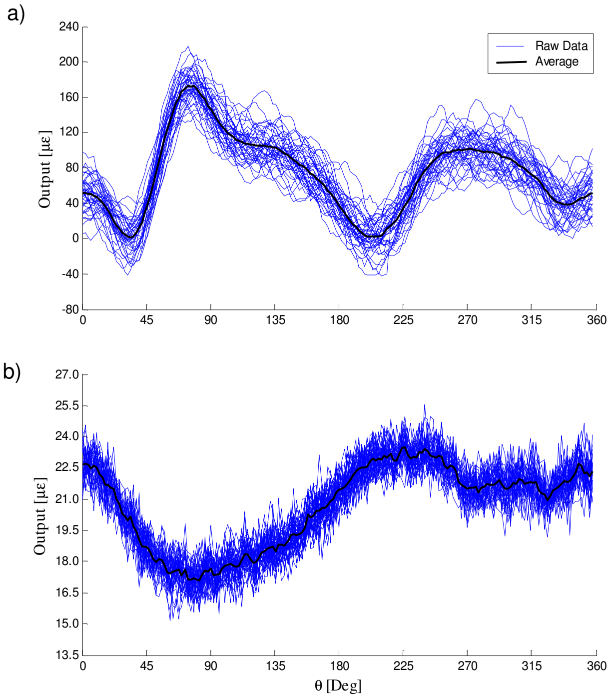

Figure 13: Without cables. (a) mid-strut bending moment sensor, (b) tension sensor (U_{wind}=8 m/s, ω=79 RPM, λ=1.45)

Finally, for blade speed ratios greater than 1.8, resonance is avoided (Fig. 11b) and the expected loading behaviour is observed. As predicted by the CFD model, dynamic stall is mainly suppressed and occurs gradually, resulting in a single large thrust peak on the upstream portion of the rotation (Refer to Fig. 2).

As previously discussed, a number of test cases were run with the cable support system in place in order to determine the effect of a change in the primary whirling frequency of the turbine as well as the emergence of higher mode natural frequencies. The PSD of the sensor outputs with the cables attached and a wind tunnel flow velocity of 8 m/s are shown in Fig. 14. Again, the support struts appear to be sensitive to a single structural mode occurring under this configuration at a frequency of 8.3Hz. In this instance however, due to the small change in natural frequency, resonance occurs at slightly different rotational velocities than without the cables. As such, high vibration response now occurs at 71 RPM and 123 RPM, or λ=1.3 and λ=2.25 respectively. However, due to relatively low vibration excitation at λ=1.1 and λ=1.8, these strain measurements can be used in place of the high vibration data sets obtained without the cable system in place.

The natural progression in the maximum thrust location is continued in the λ=1.1 mid-strut bending strain measurement, occurring at an angle of rotation of 74° (Fig. 15). As was the case for λ=0.7, this test case exhibits a series of low amplitude fluctuations in thrust loading on the downstream portion of the rotation as it is predicted that a number of small vortices are shed from the airfoil surface. The tensile strain measurement for the test case with cables closely resembles that of the test case without cables and as such has been omitted (Refer to Fig. 12b).

For λ=1.8 the maximum thrust value is reached within the expected range at θ=86°. However, by inspecting the overall trend of the data output it appears that to some small degree the resonance response of the turbine may have still been excited.

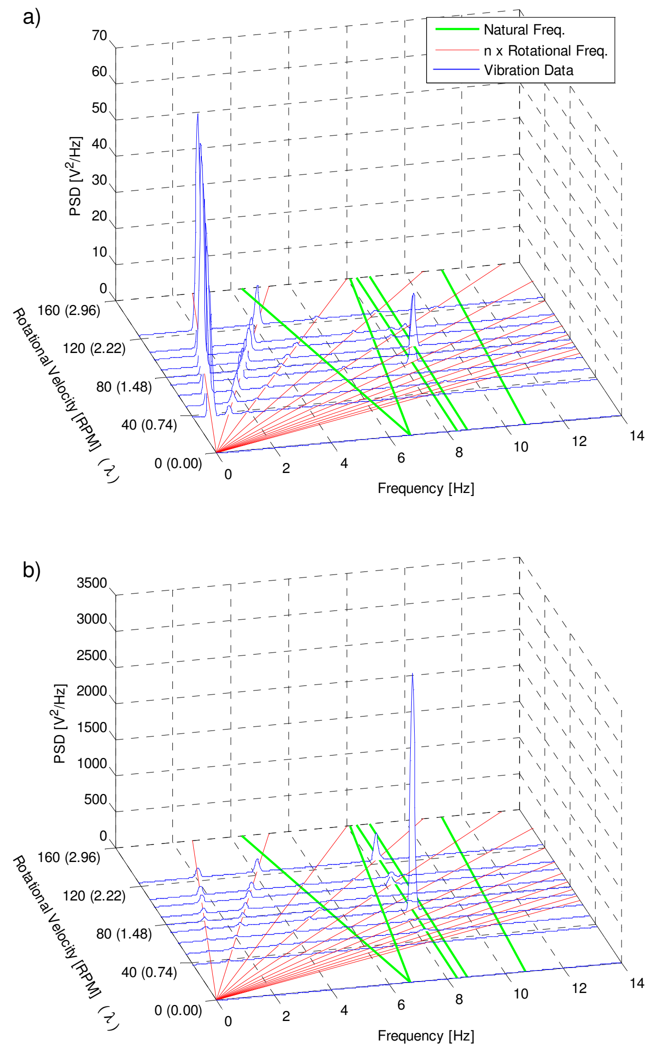

Figure 14: Power spectral density of the raw sensor data with cables as a function of rotational velocity for a flow velocity of 8 m/s. (a) tension sensor, (b) mid-strut bending moment sensor.

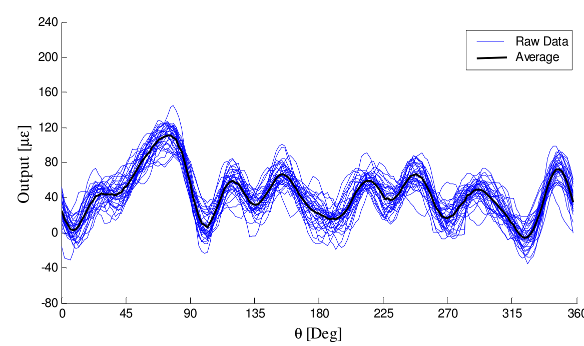

Figure 15: Mid-strut bending moment sensor with cables (U_{wind}=8 m/s, ω=60 RPM, λ=1.1)

As a confirmation of the sensor output, a number of tests were performed at various flow velocities up to 11 m/s. By normalizing the strain by the product of the dynamic pressure and the planform area of the blade ($^1/_2\rho U_{wind}{}^2cH$) the effect of a change in flow velocity could be appropriately accounted for. Note that defining the output in this way allows for direct comparison of the vibration response at a fixed blade speed ratio over a range of wind velocities, where the non-dimensionalized aerodynamic wind loading is the same, but the rotational velocity, and thus the excitation frequency, is different.

Figure 16 contains the normalized plots of the mid-strut bending moment and tension sensors for 8, 10 and 11 m/s, none of which display strong resonance characteristics. While the agreement between the bending moment sensors is quite good on the upstream portion on the rotation where aerodynamic loading is highest, some discrepancies can be seen on the downstream portion of the rotation. Despite the fact that all of the data sets displayed little response to the dominant natural frequencies of the turbine, some influence of the structural modes can still be seen in each of the mid-strut sensor outputs. The tension sensor output however indicates very good agreement between test cases. The mean offset of the three tension signals due to the difference in rotational velocity at which the data was recorded, and thus the magnitude of the applied centrifugal forces, has been accounted for.

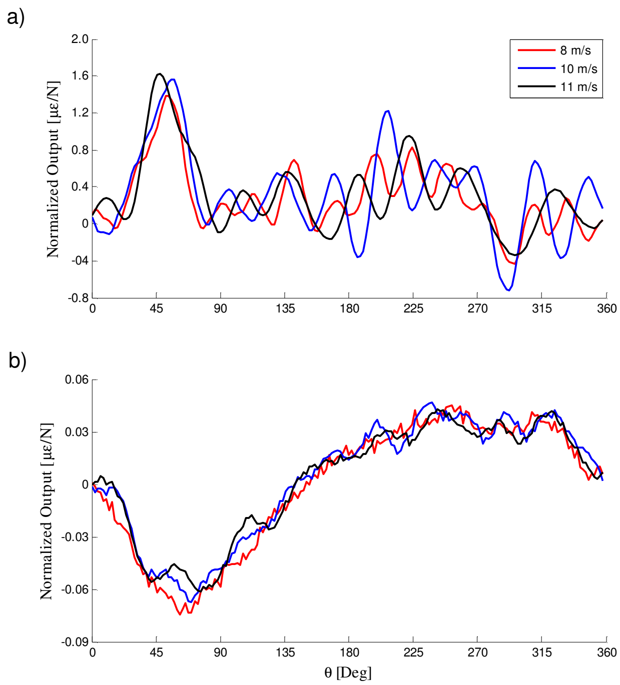

Figure 16: Mid-strut (a) bending moment sensor, and (b) tension sensor output, with cable system attached normalized by dynamic pressure force, λ=0.7.

Through a set of calibration coefficients, the above bending and tension strains can be converted into thrust and radial loads and compared with the CFD model results. However, because the objective of this research is to determine the vibration response of the turbine and its effect on obtaining measurements free from resonance, the results of this study are not included here. At present, the CFD model results are used primarily as an indication of the location of dynamic stall onset, expected loading frequencies and relative amplitudes. Furthermore, converting the strains into forces introduces additional sources of error. By considering the strains directly, the errors are limited to the accuracy of the strain gauges (±1% each) and the sampling resolution (0.3% full scale).

Beating Phenomenon: Under nearly all test conditions vibration amplitude within the support struts was observed to change dramatically during a single test run. As an example, two test cases have been selected and the mid-strut bending strain measurements have been provided below. The first case shown in Fig. 17 is a clear example of classical beating in that the modulation in amplitude occurs over a short repeatable interval. Note that 3 beating intervals have occurred over 4 rotations of the turbine. It is postulated that the reason for this beating phenomenon is the close proximity of the many strut modes. In addition, because each of the struts is manually fastened to the turbine shaft and blades, small differences in alignment and bolt tightening torques could result in variations in the stiffness of each of the six turbine struts.

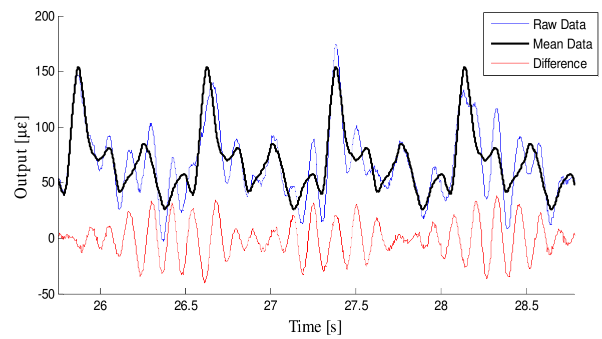

Figure 17: Sensor output for the strain gauge Wheatstone bridge mounted at the mid-point of the strut with the cable system attached. Four revolutions are shown for a typical case with classical beating (U_{wind}=8 m/s, ω=79 RPM, λ=1.45)

The second example is quite different in that the periods of low and high amplitude vibration last for considerably longer durations. Figure 18 plots the response of the mid-strut bending moment sensor for two, 4 rotation segments of data obtained within the same 30 second data sample. From approx. 18.8 to 21 seconds the vibration amplitude is low and a relatively consistent measurement signal is acquired (Fig. 18a).

However, from approx 21.6 to 24 seconds, just 1 full rotation later, the vibration amplitude has increased considerably and the mean loading signal is hard to identify (Fig. 18b). The duration of the high and low amplitude vibration periods is irregular and inconsistent; however they typically last for a total of five rotations or more. While the exact mechanism for this response is unknown, one possible explanation is that the vibration is moving between sets of airfoil struts. This would imply that for short periods of time while one or two of the blades are vibrating, the remaining blades are relatively free of vibration.

While not exclusive to all cases, it appears that the classic beating phenomenon is more likely to occur for cases with the cables attached, when the system damping is low. In contrast, cases that exhibit the more irregularly spaced high amplitude vibration response typically occur without the cables attached.

Ultimately, the many closely spaced natural frequencies in the range of 6.3 to 9.7 Hz means that resonance excitation of a structural mode is highly likely over a very broad range of rotational velocities.

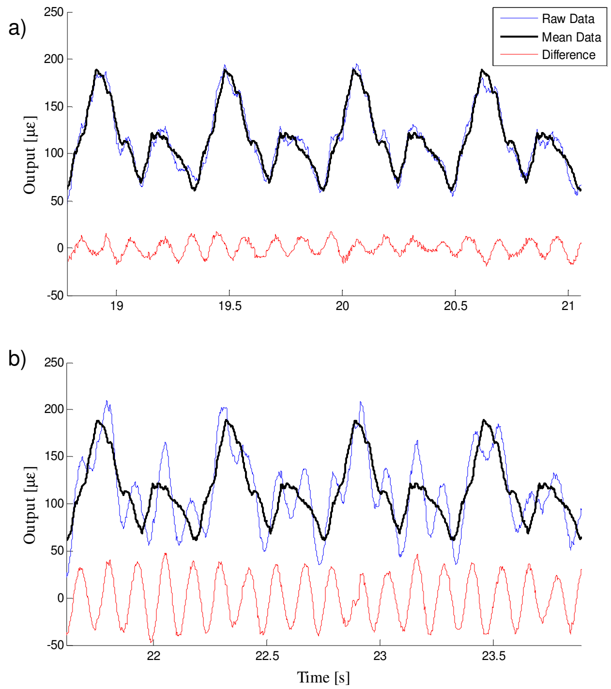

Figure 18: Sensor output for the strain gauge Wheatstone bridge mounted at the mid-point of the strut without the cable system attached. Four revolutions are shown for a typical case with intermittent vibration. (a) low amplitude vibration, (b) high amplitude vibration (U_{wind}=8 m/s, ω=106 RPM, λ=1.93).

CONCLUSION

Based upon the previous results of a series of CFD tests, the expected aerodynamic loading on the turbine was determined. This prior study indicated that the system would be subject to strong dynamic excitation, primarily at the blade pass frequency. Having identified this strong source of vibration excitation, a series of wind tunnel tests were performed to determine the vibration response of the turbine. The most observable response to dynamic excitation is clearly the large deflection in the turbine support shaft due to the primary whirling mode. By adjusting the upper end condition through the use of a cable support system an immediate increase in the frequency of this mode was realized. In addition, it was also observed that the rate at which the vibration amplitude grew in response to the blade pass frequency was greatly reduced. Furthermore, due to the asymmetry and relatively low stiffness of the base and cable support systems the emergence of a backward whirling mode was also realized.

Strain gauges mounted in the support struts provided information primarily on the presence of higher structural modes. These modes were not excited during the impact hammer tests, presumably because they are orientated in the horizontal plan and thus are not driven by deflection of the support shaft. Numerous test cases resulted in strain measurements saturated with the resonance response of the struts. It was shown that this behaviour was consistent with coincidence of integer multiples of the rotational frequency and the strut modes. In order to be able to determine what the aerodynamic loading is at all blade speed ratios, an amalgamation of the data with different shaft end conditions, and thus different natural frequencies, was performed. In addition to this, tests were also performed at various flow velocities, the results of which were normalized in such a way as to be able to make an accurate comparison. Thus, the vibration response at constant blade speed ratios where the non-dimensionalized aerodynamics wind loading is the same, but rotational velocity and excitation frequency are different, could be observed. This analysis indicated that when the aerodynamic loading is large good agreement could be found between the various wind speed results. However, the natural frequencies of the turbine still appear to have some effect on the response when aerodynamic loading is low. In general, it was observed that low blade speed ratio test cases were susceptible to high integer multiples of the rotational frequency, while intermediate to high blade speed ratio test cases were particularly vulnerable to lower integer multiples of the rotational frequency. This is an important finding as this suggests that a single natural frequency could be excited over the entire operating range of the turbine. Furthermore, under normal operating conditions the turbine is expected to be mounted on a tower structure without a guy wire support system. Typically this will reduce the system stiffness, lower the turbine natural frequencies, and compound the issues encountered in the present study.

Finally, the existence of both classical beating as well as intermittent vibration loading was also observed. It appears that this behaviour is primarily influenced by the proximity of the bending modes of the turbine struts. However, it may also come as a result of the inadvertent tuning of the struts to slightly different frequencies as a result of variable mounting stiffness.

ACKNOWLEDGMENTS

The authors would like to acknowledge the funding and support of Cleanfield Energy, the Ontario Centres of Excellence (OCE), and the Natural Sciences and Engineering Research Council (NSERC).

REFERENCES

[1] Veers, P. S., 1983, “A General Method for Fatigue Analysis of Vertical Axis Wind Turbine Blades,” Technical Report No. SAND82-2543, Sandia Laboratories, Albuquerque, NM.

[2] Oler, J. W., Strickland, L. H., Im, B. J., and Graham, G.H., 1983, “Dynamic Stall Regulation of the Darrieus Turbine,” Technical Report No. SAND83-7029, Sandia Laboratories, Albuquerque, NM.

[3] Vittecoq, P., and Laneville, A., 1983, “The Aerodynamic Forces for a Darrieus Rotor with Straight Blades: Wind Tunnel Measurements,” Journal of Wind Engineering and Industrial Aerodynamics, **15**, pp. 381-388.

[4] Paraschivoiu, I., 2002, *Wind Turbine Design with Emphasis on Darrieus Concept,* Polytechnic International Press, Montreal, Canada, pp. 177-184.

[5] McLaren, K. W., Tullis, S., and Ziada, S., 2009, “Computational Fluid Dynamics Simulation of the Aerodynamics of a High Solidity, Small Scale Vertical Axis Wind Turbine,” Submitted to Wind Energy (Manuscript # WE-09-0114).

[6] Fiedler, A. J., and Tullis, S., 2009, “Blade Offset and Pitch Effects on a High Solidity Vertical Axis Wind Turbine,” Wind Engineering, **33**(3), pp. 237-246.

[7] Howell, R., Qin, N., Edwards, J., and Durrani, N., 2010, “Wind Tunnel and Numerical Study of a Small Vertical Axis Wind Turbine,” Renewable Energy, **35**, pp. 412-422.

[8] Devaud, C. B., Weisinger, J., Johnson, D. A., and Weckman, E. J., 2008, “Experimental and Numerical Characterization of the Flow Field in the Large-Scale UW Fire Research Facility,” International Journal of Numerical Methods in Fluids, **60**(5), pp. 539-564.

[9] Den Hartog, J. P., 1956, *Mechanical Vibrations*, McGraw-Hill Book Company, Inc., New York, US, Chap. 6.

[10] Rao, J. S., 2000, *Vibratory Condition Monitoring of Machines*, Narosa Publishing House, New Delhi, India, pp. 163-174.

